Dalton Transactions

Accepted Manuscript

ROYAL SOCIETY OF CHEMISTRY

rsc.li/dalton

Cite this: DOI: 10.1039/c0xx00000x

www.rsc.org/xxxxxx

ARTICLE TYPE

Ag@Au nanoprisms-metal organic frameworks-based paper for extending glucose sensing range in human serum and urine

Pin-Hsuan Huang,[a] Chia Ping Hong,[a] Jian Fan Zhu,[a] Tzu-Ting Chen,[a] Chu-Ting Chan,[a] Yu-Chien Ko,[a] Tien-Li Lin,[a] Zheng-Bang Pan,[a] Ning-Kuei Sun,[a] Ying-Chu Wang,[a] Jong-Jheng Luo,[a] Tzu-Chieh Lin,[b] Chia-Cheng Kang,*[b] Jing-Jong Shyue*[c] and Mei-Lin Ho*[a]

Received (in XXX, XXX) Xth XXXXXXXXX 20XX, Accepted Xth XXXXXXXXX 20XX
DOI: 10.1039/b000000x

In this work, we present a Ag@Au nanoprism-metal-organic frameworks-paper based glucose sensor for rapid, sensitive, single-use and quantitative glucose determination in human serum. To achieve painless measurement of glucose with a non-invasive detection methodology, this biosensor was further tested in human urine. In this approach, a new hybrid-Ag@Au nanoprisms loaded in close proximity to micrometer sized coordination polymers as phosphorescent luminophores significantly enhanced the emission intensity due to metal-enhanced phosphorescence and worked as reaction sites to support more dissolved oxygen. Reports of enhanced phosphorescence intensity are relatively rare, especially at room temperature. The true enhancement factor of Ag@Au-phosphorescent metal-organic frameworks on paper was deduced to be 110-fold, making it a better optical type glucose meter. The results demonstrate the validity of the intensity enhancement effect of the excitation of the overlap of the emission band of a luminophore with the surface plasmon resonance band of Ag@Au nanoprisms. Ag@Au nanoprisms were used not only to improve the detection limit of glucose sensing but also to extend the glucose sensing range by enhancing the oxygen oxidation efficiency. The oxidation of glucose as Glucose oxidase is accompanied by oxygen consumption, which increases the intensity of the phosphorescence emission. The turn-on type paper-based biosensor exhibits a rapid response (0.5 s), a low detection limit (0.038 mM), and a wide linear range (30 mM to 0.05 mM), as well as good anti-interference, long-term longevity and reproducibility. Finally, the biosensor was successfully applied to the determination of glucose in human serum and urine.

Introduction

The development of monitoring tools for glucose is important.[1,2] Such tools would allow healthy people to diagnose and track possible factors that affect glucose levels, and people with diabetes further to manage the disease. Owing to the growing prevalence of diabetes, optical technologies using photoluminescence have attracted increasing attention.[3] The promising features of photoluminescence-based glucose sensors over conventional electricity-based meters are numerous. They are simple in design, low in cost, non-destructive, sensitive, and free from electrical and magnetic disturbances. They also require no work with flammable/explosive compounds or reference cells, and they have the potential for non-invasive glucose monitoring.[4-5] Furthermore, unlike colorimetric strips, luminescence can be measured not only by its intensity but also its lifetime. Hence, such technologies can further provide important information about the biomolecular structures and environments associated with healthy and diseased states.[3]

Numerous fluorescent luminescent materials have been used for glucose detection, including alizarin red,[7] anthracene,[8] coumarin-NH_2,[9] naphthalene-sulphonuc acid derivative,[10] CdS QDs derivative,[11] Concanavalin A (Con A),[5] glucose binding protein,[5] and boronic acid derivatives,[5] but phosphorescence-based materials, as compared to the developed fluorescent materials, are quite few in number.[12-17] Recently, some reports have described the application of nanomaterials in combination with dye molecules for optical glucose detection.[18-20] Nanomaterials facilitate optical glucose sensing because they offer advantages such as a large surface area,[21] enhanced catalytic activity,[18] and enhancement of the luminescence intensity of luminophores.[3]

Among all nanomaterial types, noble metal nanoparticles (e.g., Au and Ag NPs) have good affinity to biomolecules[18] and exhibit many unique electronic and optical properties,[22] such as strong surface plasmon resonance absorption,[23,24] enhanced electromagnetic fields, and size-dependent quantum confinement effects.[22] Moreover, the surface plasmon resonance absorption of metal NPs having anisotropic shapes, e.g., Ag nanoprisms, is even stronger than that of spherical ones, leading to an enhanced absorption cross-section and thus increased detection sensitivity.[23,24] Among the various noble metal NPs, Ag and Au nanostructures are the best candidates for enhancing

View Article Online
DOI: 10.1039/C7DT00875A

luminescence due to their surface plasmon absorption bands in the visible range. Here we report a new hybrid nanoparticle geometry that combines the plasmonic properties of both an isotropic nanoprisms (Ag) and isotropic nanospheres (Au), namely, Ag@Au nanoprisms, in a single structure, and exhibits promising potential. This Ag@Au nanoprism is composed of a triangular Ag nanoprism decorated with Au nanospheres.

When dye molecules are adsorbed onto the surfaces of noble metal NPs, their luminescence intensity is enhanced or quenched depending on several factors, including the distance between the NPs and luminophore, the shape of the NPs, the orientation of the luminophore, spectral overlap between the plasmon resonance of the NPs, and the excitation and/or emission spectra of the luminophore.[25,26] When emission intensity is enhanced, this phenomenon is called metal-enhanced luminescence. To date, much work has focused on metal-enhanced fluorescence.[27] However, another surface plasmon coupled luminescence phenomenon, metal-enhanced phosphorescence (MEP), offers additional applications.[28,29]

In this work, the resulting Ag@Au nanoprism structures exhibited greater luminescence than did pure Ag nanoprisms. Moreover, the possible effects of these noble metal nanoparticles on the sensitivity, reproducibility, and stability of coupled phosphorescent metal-organic frameworks remains an interesting issue, as such effects may offer/regulate the probe potential against glucose detection. A MEP system is designed for the quantitative analysis of glucose by conjugating rough Ag@Au heterometallic nanoprisms to act as not only an expanded platform to support more oxygen adsorption but also as a reaction site. At the same time, Ag@Au nanoprisms in close proximity to a luminophore significantly enhance the phosphorescence emission intensity and thus improve the detection limit of glucose sensing. The overall fabrication process is illustrated in Scheme 1. A fixed region of wax is stamped onto a paper substrate to ensure that the glucose solution penetrates through the fixed area. Rough Ag@Au heterometallic nanoprisms are synthesized and dropped onto the paper. Ir-Zn_e metal-organic frameworks (MOFs) are used as luminophores due to their noteworthy oxygen-sensing properties and shorter response and recovery times toward oxygen.[30] The oxidation of glucose at GOx (Glucose oxidase) is accompanied by oxygen consumption, which increases the intensity of phosphorescence emission. This new approach allows low-volume sampling, a fast response, miniaturization, portability, disposability, sensitive detection, and an extended glucose sensing probe. Compared to regular paper-based glucose optical sensors, our method extends the linear sensing range and can be used for clinical analysis and disease diagnosis.

Results and Discussion

Design of paper-based biosensor

In this design, in order to obtain the greatest enhancement of luminescence intensity and hence expand the response range toward glucose, Ag nanoprisms (which have a greater excitation enhancement factor than Au spheres and Ag cubes)[26] and Au nanosphere composite structures were built. As shown in Scheme 1, Ag@Au nanoprisms were added into the paper (Ag@Au nanoprisms on paper). Then phosphorescent Ir-Zn_e MOFs were superimposed on nanoprisms (Ag@Au-Ir–Zn_e MOFs on paper)

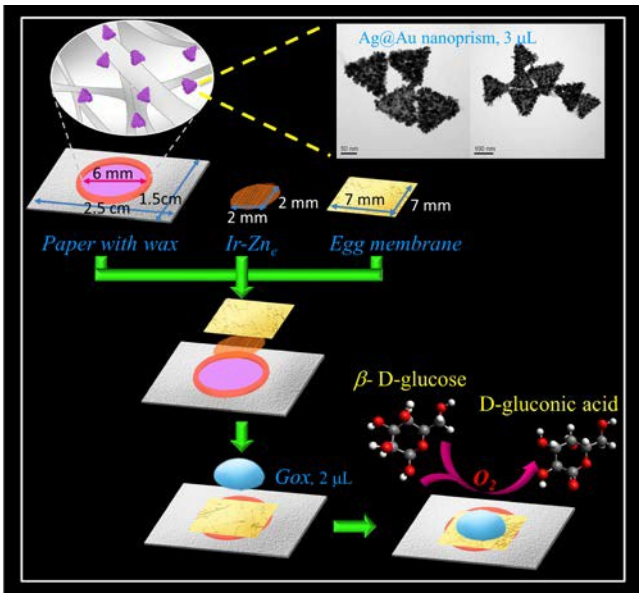

Scheme 1. Schematic illustration of the fabrication process and sensing mechanism of Ag@Au nanoprisms-metal organic frameworks based paper for glucose sensing.

as illustrated in Scheme 1 (and also Scheme S1 in the supporting information). Upon excitation of the luminophores, i.e., Ir-Zn_e MOFs, the coupling of the MOF dipoles with the localized electromagnetic field of Ag@Au nanoprisms increased the absorption cross section[27] and the emission intensity enhancement of the MOFs. At the same time, Ag@Au nanoprisms shaped like the onigiri of Chinese/Japanese food were used to increase the surface area and thereby to provide opportunities for enhancement of the efficiency of the catalytic performance, and also to provide environments for oxygen-capping. Next, when the glucose was added, oxygen molecules in the interior of the biosensor were quickly and efficiently consumed by the GOx. As a result, the phosphorescence intensity of Ir-Zn_e MOFs was fast and significantly enhanced.

Characterization of Ag@Au nanoprisms and Ir-Zn_e

The TEM images in Scheme 1 and EDX mapping in STEM mode (Figure 1 (a)-(d)) demonstrated that spherical Au nanoparticles were deposited and nucleated on the Ag nanoprisms, i.e. Au extended further out than Ag in the merged mapping in Figure 1(d) (hence Au on Ag). Furthermore, owing to the higher atomic weight and stronger scattering, the darker contrast correlated to the Au mapping at the edges of the Ag nanoprisms also indicated the Au is on the Ag. The sizes of the Ag@Au nanoprisms and Au nanoparticles were determined by TEM (Hitachi H-7100). Further information was provided by the histogram analysis (see Supporting Information, Figure S1), the results of which indicated that the average edge length of Ag@Au nanoprisms was about 128.9 ± 35.3 nm, and the average particle size of Au was about 12.61 ± 2.55 nm. Note that the histogram regarding the particle size distributions of Ag@Au nanoprisms and Au nanoparticles was constructed on the basis of six TEM photographs, and a total of ~60 prisms (~160 particles) were used in this histogram.

Optical and SEM images of Ir-Zn_e MOFs obtained at 5V and 30 ^{o}C for 1 h are presented in Figure S2. The morphology was

View Article Online
DOI: 10.1039/C7DT00875A

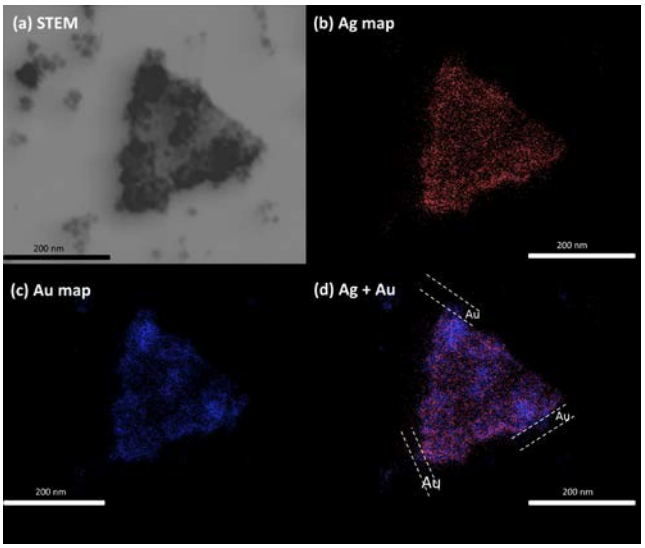

Figure 1. (a)–(d) STEM images in bright-field mode and the elemental maps of Ag@Au nanoprisms.

micro-plates, and the average size was about 7.8 μm. Based on our previous report,[30] compound Ir-Zn_e consists of $Ir(ppy)_2(H_2dcbpy)PF_6$ (L-H_2, ppy = 2-phenylpyridine, H_2dcbpy = 4,4'-dicarboxy-2,2'-bipyridine) ligands coordinated to a Zn center *via* carboxylate groups. The basic building unit of Ir-Zn_e is composed of a four-coordinate Zn(II) center bonded with four oxygen atoms from four carboxylate groups of L ligand, and is configured in a distorted tetrahedral geometry. The L ligand adopts a bis-monodentate bridging mode connecting the Zn(II) centers, constructing one-dimensional chains. The adjacent chains are then mutually interlinked to the 3D structure.[30] The emission from ^{3}MLCT (metal to ligand charge transfer) excited state has been observed.

Optical properties of biosensors and optimization of the volume and concentration of Ag@Au nanoprisms

The corresponding optical properties of Ir–Zn_e MOFs on paper, small and big Ag nanoprisms in solution, Ag@Au nanoprisms in solution and on paper, and Ag@Au-Ir–Zn_e MOFs on paper were revealed by the UV-vis spectra and emission spectra (Figure 2 and Figure 3). As shown in Figure 2, the UV-vis spectrum of small Ag nanoprisms was characterized by one sharp peak and two lower-lying broad absorption bands with maxima at 337, 445, and 620 nm, respectively, which have been ascribed to the out-of-plane quadrupole, in-plane quadrupole, and in-plane dipole plasmon resonances.[31] As the smaller Ag nanoprims transformed into bigger ones, red-shift in the in-plane quadrupole and in-plane dipole plasmon resonances was observed.

The absorption spectrum of Ag@Au nanoprisms in solution (Figure 2) and on paper (Figure 3) exhibited a broad peak around 522 nm, which is attributed to the surface plasmon resonance of Ag@Au nanoparticles.[32] As compared to the spectra of Ag@Au nanoprisms, the maximum absorption of Ag@Au-Ir–Zn_e MOFs increased and broadened, suggesting the coupling of dipoles between Ag@Au nanoprisms and Ir–Zn_e MOFs, and an increase in the absorption cross section of Ir–Zn_e MOFs.[33]

The suitable volume and concentration of Ag@Au nanoprisms allowed precise optimization of the emission intensity

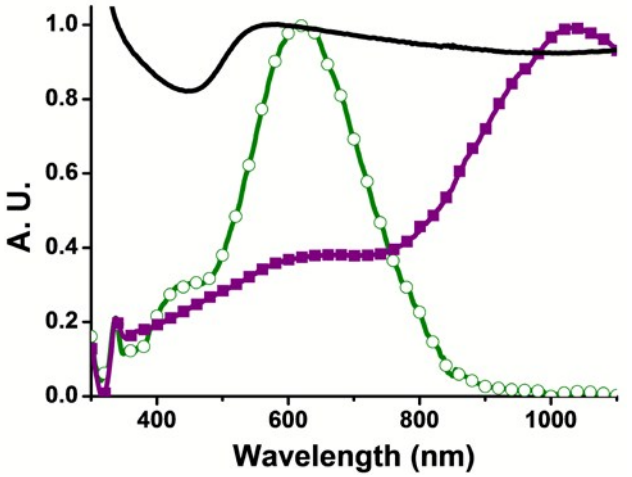

Figure 2. The absorption of small Ag nanoprisms (olive,-○-), big Ag nanoprisms (purple,-▩-), and Ag@Au nanoprism (black) in solution.

enhancement. Data were obtained from the average value of three measurements. The influence of Ag@Au nanoprism volume and absorbance on the extent of MEP is shown in Figure S3 and S4, where the intensity enhancement is shown to rise rapidly when the volume and absorption of Ag@Au nanoprisms is 3 μL and λ_{abs} = 0.013 at 522 nm (in 10 mL DI water). This result can be plausibly explained by an increase in the efficiency of the energy transfer between the MOFs and nanoprisms through-space as the amount of Ag@Au nanoprisms increases (MEP). Alternatively, as the concentration of Ag@Au nanoprisms further increases, the energy transferred from the luminophore to the Ag@Au nanoprisms can be re-scattered back into the far-field by Ag@Au nanoprisms, or the energy of the excited luminophore can be quenched by loss to non-radiactive decay pathways, e.g., absorption, in the Ag@Au nanoprisms.[26] Accordingly, this luminescence quenching under the higher concentration of Ag@Au nanoprisms can be ascribed to the scattering and absorption effect caused by Ag@Au nanoprisms. Also, note that the thickness of filter paper is 0.22 mm; we assume that when the Ag@Au nanoprism solution was dropped to the filter paper, the nanoprisms distributed within this depth. Because MOFs are attached to the surface of the filter paper, this luminescence quenching phenomenom is hence related to a long-distance (far-field) quenching mechanism that is unlike the short-distance (near-field) quenching of Föster resonance energy transfer.[34]

As shown in Figure 3, the absorption and emission peaks of MOFs have spectral overlap with the localized surface plasmon resonance scattering peak of Ag@Au nanoprisms. When the incident light, i.e., 532 nm, excited MOFs where non-radiative energy transfer occurred from the excited MOFs to the surface plasmon electrons in Ag@Au nanoprisms, the surface plasmons in turn radiated MOFs emission. Moreover, as indicated by Munechika *et al.*,[26] brighter luminescence can be observed when the emission peak of the luminophore is at lower energy, e.g. 532 nm, relative to the localized surface plasmon resonance scattering peak of NPs. This can be rationalized; when the surface plasmon resonance of NPs matches the luminophore emission, both the radiative and non-radiative decay rates are enhanced, which is disadvantageous in terms of luminesence intensity.

From Figure 3, for the control test, the enhanced emission

View Article Online
DOI: 10.1039/C7DT00875A

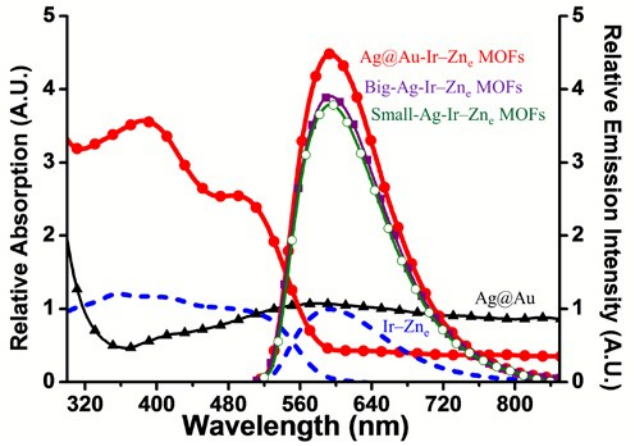

Figure 3. Absorption and emission spectra at room temperature of Ir–Zn$_e$ MOFs (blue,---) and Ag@Au-Ir–Zn$_e$ MOFs on paper (red,- ● -), absorption spectra of Ag@Au nanoprisms on paper (black,-▲-), emission of big Ag-Ir–Zn$_e$ MOFs on paper (purple, -▩-) and small Ag-Ir–Zn$_e$ MOFs on paper (olive,-○-).

intensities of big Ag nanoprisms and small Ag nanoprisms capped with Ir-Zn$_e$ (big Ag-Ir–Zn$_e$ MOFs and small Ag-Ir–Zn$_e$ MOFs) were 3.9- and 3.8-fold, respectively, as compared to Ir–Zn$_e$ MOFs only on paper, where big Ag nanoprisms and small Ag nanoprisms had the same absorption as the Ag@Au nanoprisms around 522 nm. If the more concentrated big Ag nanoprisms and small Ag nanoprisms were used, the enhanced emission intensities decreased to < 3-folds. An 4.5-fold increase in the phosphorescence emission intensity of Ag@Au-Ir–Zn$_e$ MOFs on paper upon excitation at 532 nm at room temperature was obtained, as compared to Ir–Zn$_e$ MOFs on paper. The absorption around 532 nm increased by 1.9 fold when Ir-Zn$_e$ MOFs were attached to Ag@Au nanoprisms, while emission intensity increased by more than 4.5 times, suggesting that the energy absorbed by Ag@Au nanoprisms was transferred efficiently to MOFs, increasing the emission intensity. Note that for most of the phospher, the quantum yield was relatively small at room temperature due to collisional deactivation by oxygen and thermal quenching. In this regard, the luminescence of Ag@Au-Ir–Zn$_e$ MOFs on paper could easily be observed by the naked eye due to the MEF effect.

In our system, the MOFs were not attached to the Ag@Au nanoprisms efficiently because the longest distance between MOFs and nanoprisms was up to a micrometer (*vide supra*). Although we sacrificed the distance control of the experiments, the excitation enhancement factors, i.e., the spectral overlap between the localized surface plasmon resonance peaks of nanoprisms and absorption/emission of MOFs, were large enough to enhance the luminescence intensity of Ag@Au-Ir–Zn$_e$ MOFs on paper and allow us to estimate the enhancement factors.

Reports of enhanced phosphorescence intensity are relatively rare, especially at room temperature. Phosphorescence intensity enhancement of ~5.7 fold at 77K has been reported by the Geddes research group.[29] Based on their work, the true enhancement factor of Ag@Au-Ir–Zn$_e$ MOFs on paper at room temperature was therefore deduced to be 110-fold, making it a better optical type glucose meter.[29] The results demonstrate the validity of the intensity enhancement effect of the excitation of the overlap of the emission band of a luminophore with the surface plasmon resonance band of Ag@Au nanoprisms.

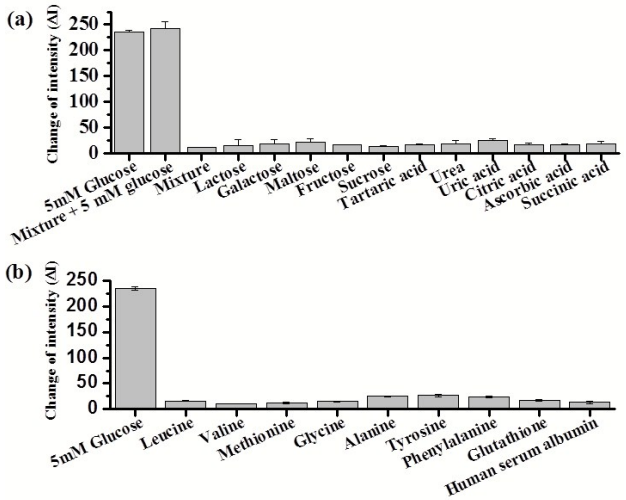

Figure 4. (a) Interference test of the glucose biosensor at pH 7.0 PBS buffers. (b) The influences of common substances present coexisting in serum/urine. Note, the mixture contained all of the interfering substances, including substances in blood or urine or coexisting in serum/urine.

Using the optimized conditions of Ag@Au-Ir–Zn$_e$ MOFs on paper, the effects of concentration and pH value of buffer solution were subsequently examined in the following glucose-sensing experiments. The effects of concentration and pH value of the buffer solution on the further luminescence intensity enhancement upon the addition of 5 mM glucose with 10 mg/mL GOx was examined by applying buffer solution with concentrations of 50, 100, 125, 150, 175, and 200 mM, and pH values of 6-8 for conditioning, respectively. As shown in Figure S5, the concentration with 175 mM exhibited the strongest phosphorescence enhancement effect. We suggest that the higher concentration of buffer caused conformation changes of the enzyme to make more oxygen accessible in this case. This higher buffer concentration also stabilized the pH value to 7 (Figure S6), thus keeping the enzyme activity at its maximum.

Optimization of concentration of GOx and the volume of calcium chloride

In order to find the most suitable concentration of GOx, the extent of the enhancement of the intensity in the system was studied. It was found that the emission intensity increased as the enzyme concentration was increased, reaching its maximum at 14 mg/mL (Figure S7). The increase in emission intensity was probably due to more oxygen being accessible under the Ag@Au nanoparticle environmental condition (i.e., reaction sites), and therefore more GOx being consumed.

Subsequently, the content of calcium chloride in the system was optimized, as shown in Figure S8. The calcium chloride in the system slowly cross-linked the alginate for the thickening, stabilizing, and gel-forming of GOx. The range of content was from 0 to 50 mmol. It can be seen that the maximum enhanced phosphorescence intensity was achieved with a content of 10 mmol.

Selectivity against interference

View Article Online
DOI: 10.1039/C7DT00875A

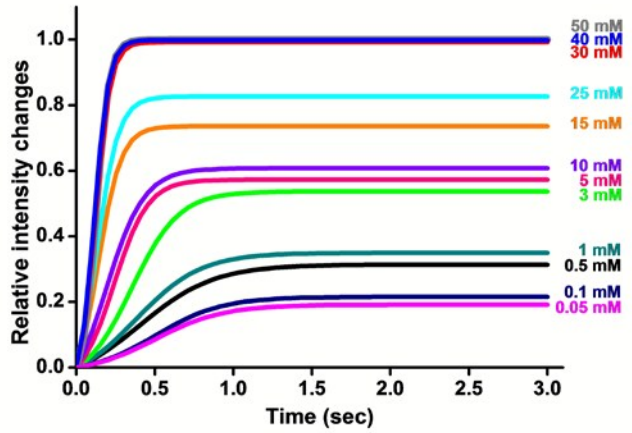

Figure 5. Relative emission intensity change curves of paper-based biosensor upon addition of different concentrations of glucose.

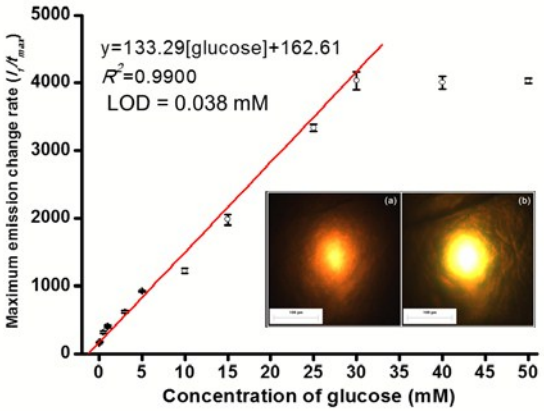

Figure 6. Maximum emission change rate–glucose concentration calibration curve obtained for the paper-based biosensor. Inset: luminescence changes ((a) and (b)) of the sensor upon addition of 30 M glucose: (a) before addition, (b) after addition. Scale bar is 100 μm.

The influences of common substances present in blood or urine (Figure 4(a)) or coexisting in serum/urine (Figure 4(b)) were tested individually and in mixtures to investigate the selectivity of the system for glucose determination. The concentrations of the potential interfering substances were 10 mM, and the concentration of human serum albumin was 0.075 mM (saturated concentration). Figure 4 shows the relative intensity increases of Ag@Au-Ir–Zn_e MOFs on paper with different substances. It was observed that none of the investigated substances, even in mixtures of all agents, caused notable effects on the intensity of the biosensor. However, when 5.0 mM glucose solution was added to the interferents, the increase in intensity was apparent. Therefore, as a specific probe for diabetes diagnosis, this paper-based sensor design takes advantage of the high specificity for glucose by using GOx.

Paper-based biosensor for glucose detection

On the basis of the above results, we selected the optimized conditions to assemble Ag@Au nanoprisms on paper for glucose sensing detection. Figure S9 shows the relative changes in emission intensity of MOFs (without Ag@Au nanoprisms) on paper, of small and big Ag-Ir–Zn_e MOFs, and Ag@Au-Ir–Zn_e MOFs on paper upon exposure to 3 mM glucose. As shown in Figure S9, the relative intensity enhancement of small Ag-Ir–Zn_e MOFs, big Ag-Ir–Zn_e MOFs, and Ag@Au-Ir–Zn_e MOFs were larger than that of MOFs only. Also, we found that the time point of inflection (t_{max}) in the curve, i.e. where the maximum rate of phosphorescence intensity increase, of pure MOFs < Ag@Au-Ir–Zn_e MOFs < small Ag-Ir–Zn_e MOFs < big Ag-Ir–Zn_e MOFs. The introduced nanoparticles provide a better sensing behavior toward glucose than MOFs only can be attributed to the surface of Ag nanoprisms or Ag@Au nanoprisms, which allows the enzyme molecules having more freedom of orientation to close to the particle surface, and thus promotes the active site of the glucose oxidase to the MOFs.[35] Meanwhile, the surface of Ag nanoprisms or Ag@Au nanoprisms provides more glucose oxidase to distribute,[36] leading to increased collision opportunity with oxygen, and hence results in the increase of intensity. The results also clearly indicate that Ag@Au nanoprisms generated an enhanced local electromagnetic field to increase luminescence intensity and that oxygen molecules were more efficiently consumed by the GOx on Ag@Au nanoprisms than by MOFs alone.

As shown in Figure 5, when the glucose concentration was increased from 0.05 mM to 50 mM, the change in emission intensity was gradually elevated. The response saturation point of all curves was reached when oxygen molecules were exhausted within 0.5 sec. The maximum emission change rate (I_1/t_{max}) upon the addition of different glucose concentrations was further calculated based on eqn (1) for the quantitative analysis. For each concentration, the maximum emission change rate was plotted against glucose concentration, as shown in Figure 6. There was a good linear correlation in the range of 0.05-30 mM (y = 133.29 [glucose] + 162.61, R^2 = 0.9900). The detection limit was 0.038 mM from three times signal to noise.

$$I_t = I_1 + \frac{I_0 - I_1}{1 + e^{(t - t_{max})dt}}$$

$$Rate = \frac{I_1}{t_{max}} \quad (1)$$

When the concentration of glucose was above 30 mM, the maximum emission change rate gradually reached saturation because the oxygen was used up by GOx; afterward, no changes in emission intensity occurred. The change in luminescence intensity before/after the addition of glucose could easily be distinguished with the naked eye (Inset of Figure 6). It is worthy of note that this biosensor exhibited excellent performance for glucose sensing in terms of the linear response range and the response time as compared to previously reported optical biosensors supported by nanomaterials, as listed in Table S1.[20]

The linear range of this biosensor (2-30 mM) was much wider and thus suitable for diagnosing patients with diabetes and for monitoring glucose in the blood (4.4-6.6 mM) and urine (0.1-0.8 mM) of healthy persons.[37-39] Additionally, as shown in Table S1, most of the previous publications on the use of nanomaterials for optical sensing of glucose have focused on the detection of short-lived fluorescence quenching/enhancement or phosphorescence quenching phenomena. However, this detection method may

View Article Online
DOI: 10.1039/C7DT00875A

Table 1. Detection of glucose in human serum.

Human Serum	Concentration (mM)		Glucose added (mM)	Glucose found[a] (mM)	Recovery (%)	R.S.D.[b](%)
	Claimed value	Proposed method[a]				
Concentration 1	6.575 ± 0.094[c]	6.737 ± 0.198				2.94
2			2	2.259 ± 0.058	112.9	2.58
3			3	3.221 ± 0.040	107.4	1.25
4			4	4.127 ± 0.041	103.2	0.99
5			5	5.085 ± 0.046	101.7	0.97
Concentration 6	16.35 ± 0.20[c]	16.22 ± 0.119				0.73
7			0.5	0.566 ± 0.010	113.1	1.76
8			1	1.002 ± 0.023	104.8	2.34
9			2	1.933 ± 0.047	96.66	2.41
10			3	2.821 ± 0.089	94.03	3.16

[a] Average of three determinations.
[b] R.S.D.: relative standard deviation.
[c] The glucose concentrations in human serum were certified by the definitive method, isotope dilution gas chromatography mass-pectrometry.[41]
[d] $t_{0.05,\,2} = 4.30$.

suffer from interference by autofluorescence and light scattering of biological matrixes. Furthermore, our sensor exhibits phosphorescence-on-response upon oxidation of glucose by GOx, a wider linear response range, lower LOD, and faster response time, and it is easy to observe with the naked eye, making it superior to the less sensitive "turn-off" sensors due to the lower background signal (see inset of Figure 6). Even compared with those of the Ag nanoprisms-based colorimetric system,[40] both the sensing range and response time of this biosensor are more suitable for diagnosing diabetes patients.

Analysis of human blood serum and glucose detection

To validate the application performance of the present proposed method, the phosphorescence of glucose (NIST SRM 965) in human blood serum was determined and the results were compared with those measured by a GC-MS (see Table 1). The glucose concentration in the serum was then calculated from the calibration curve in Figure 6. The concentrations of glucose in the serum samples determined by the GC-MS method were 6.575 ± 0.094 and 16.35 ± 0.20 mM, and those obtained with the optical sensing method were 6.737 ± 0.198 and 16.22 ± 0.119 mM, respectively (N = 3). A t-test performed at a 95% confidence level demonstrated that the results obtained by the two methods did not differ significantly. Analysis of the glucose of these two concentrations was precise, 2.94% and 0.73% R.S.D., respectively, indicating that the results were accurate and credible. The feasibility of our present method was further validated by standard addition experiments. The recovery of glucose from the three serum samples ranged from 94.03% to 113.1%. These results confirmed that the paper-based biosensor can be applied to actual sample analysis.

Glucose detection in human urine

To provide a non-invasive approach to glucose sensing, this biosensor was further used to determine glucose concentrations in human urine. Urine samples used in this study were obtained from a healthy man aged 20 years old. Prior to analysis, most of the proteins in the urine samples were removed, and the resulting samples were diluted ~100 folds using PBS buffer. Known concentrations of glucose were spiked into human urine by standard addition method and the response was measured. As can be seen in Table 2, the good recovery results and R.S.D values indicated that the proposed sensor can also be effectively used for urine sample analysis to detect glucose.

Storage stability

When this biosensor was not in use, it was stored in a refrigerator at 4 ºC in a humid environment. Figure S10 shows the stability curve of this biosensor. After a storage period of ~60 days, the sensor retained 98.9% of its initial response rate, indicating good storage stability.

Table 2. Determination of glucose in human urine. Data were obtained from an average value of three replicate measurements.

Human Urine	Glucose added (mM)	Glucose found (mM)	Recovery (%)	R.S.D. (%)
Sample 1	1	0.990 ± 0.025	99.00	2.52
	3	3.156 ± 0.160	105.2	5.07
	5	4.807 ± 0.023	96.14	0.48
	10	9.871 ± 0.336	98.71	3.40
	15	14.77 ± 0.826	98.47	5.59

Conclusions

In this study, we have shown that a judicious design of Ag@Au nanoprisms capped with phosphorescent MOFs can lead to dramatic enhancement of the luminescence intensity of phosphorescent MOFs. This design provides more surface area as reaction sites to collide with oxygen and optical enhancement via energy transfer, thus extending the glucose sensing range to the same range of commercial glucose meter. This biosensor exhibits rapid detection, low LOD, single-use, good storage stability, reproducibility and good anti-interference for glucose. This work also suggests that the proposed biosensor exhibits good analytical features and that the glucose determination performance in serum and urine samples is satisfactory. Accordingly, it is clear that future extension of this research using bimetallic nanoparticles or

View Article Online
DOI: 10.1039/C7DT00875A

alloys capped with MOFs for biosensing should provide versatility. Also, a better support can also be designed and co-anchored with nanoparticles-MOFs, among which a potential candidate should be chitosan on the paper surface because it can modify paper surfaces and create a more effective reactive area.[42] The resulting system is expected to be greatly expand the usefulness of biosensing.

Experimental sections

Materials and reagents

Glucose oxidase (GOx, EC 1.1.3.4 from Aspergillus Niger) with a specific activity of 1 529 80 U g-1 of lyophilized solid and D-(+)-glucose (99%) were purchased from Sigma. All solvents were obtained from commercial suppliers and were used without further purification unless otherwise noted. Phosphate buffer (pH 7.0) was prepared from 175 mM monosodium phosphate monohydrate and 175 mM disodium hydrogen phosphate (Merck). Advantec filter paper No. 5C was obtained from Toyo Roshi Kaisha, Ltd.

Preparation of Ag nanoprisms and Ag@Au nanoprisms

First, smaller Ag nanoprisms were developed based on our earlier work[31] and Mirkin *et al.*[43,44] 10 mL small Ag nanoprisms, trisodium citrate (0.4 mM, 5 mL), and L-Ascorbic acid (0.1 mM, 5 mL) solution were mixed together. Then silver nitrate (6 μM, 10 mL) was added dropwise under continuous stirring. The resulting solution was then purified by centrifugation (8,000 rpm, 10 min). The growth process of Ag nanoprisms was traced by UV-vis spectroscopy. This step was repeated several times until the corresponding absorption maximum of ~1,000 nm was achieved. The as-prepared larger Ag nanoprism solution (0.1 mL), millipore water (25 mL), sodium borohydride solution (0.1 M, 300 μL), and gold(III) chloride trihydrate (0.01 M, 15 μL) were then added into 5 mL L-Ascorbic acid (0.05 mM) under stirring for 5 min in the dark at room temperature. The sizes of the Ag nanoprisms and Ag@Au nanoprisms were determined by TEM (JEOL JEM-1230).

STEM Measurements

Elemental mapping analyses were performed with a Scanning Transmission Electron Microscope (STEM, JEOL 2100F, Japan) equipped with a Silicon Drift Detector (SDD, Oxford X-Max, UK) operated at 200 kV in bright-field mode.

Fabrication of wax-pattern paper-based analytical devices (Scheme 1)

Crystalline Ir–Zn_e MOFs were prepared by the electrochemical method described in our previous paper.[33] The Ir–Zn_e MOFs on stainless steel mesh were cut into squares (2 mm × 2 mm). The filter paper was cut into strips of 2.5 cm × 1.5 cm. Subsequently, a hollow circle column mold was used to stamp the melted wax (~5 μL) on the surface of the filter paper, followed by drying at 30 °C for 30 min to form the hydrophobic barrier. For immobilization of nanoparticles, 3 μL solution of Ag@Au nanoprisms, big nanoprisms, or small nanoprisms with absorption = 0.013 at 522 nm was dropped onto the filter paper and dried under ambient conditions (Ag@Au nanoprisms on paper, big nanoprisms on paper, and small nanoprisms on paper). Ir–Zn_e MOFs were then overlaid onto the Ag@Au nanoprisms, big nanoprisms, and small nanoprisms (Ag@Au-Ir–Zn_e MOFs on paper, big Ag-Ir–Zn_e MOFs on paper, and small Ag-Ir–Zn_e MOFs on paper), after which a 7 mm square of eggshell membrane was overlaid on it. Next, GOx (2 μL) in buffer solution was packaged into a hydrogel sphere containing 50 μL of 0.2 M calcium alginate. 5 μL of glucose standard solution or serum sample or urine was spotted onto the sphere, and the luminescence signal under irradiation at 532 nm was collected with a fiber-optic system.

Preparation of human serum, urine, and glucose solution

Human serum (SRM 965b) was obtained from NIST. The glucose concentrations, 6 mM and 16 mM, in human serum were certified by the definitive method, isotope dilution gas chromatography mass-spectrometry.[41] The resulting serum solutions were filtered using the Nanosep centrifugal device with a cut-off of 3 KDa (Omega; Pall Corp., East. Hills, NY) at 14,000 rpm and 4 ºC for 10 min. Human urine samples were collected from healthy volunteers. Samples were initially heated at 95 ºC for 20 min and then cooled to room temperature with subsequent centrifugation at 14,000 rpm for 10 min to remove most of the proteins. Finally, the filtrate was dilulted 100-fold by PBS buffer and used as the test sample. Standard glucose concentrations in buffer solution ranged from 0.50-50 mM.

Spectral measurement

For all of the glucose sensing experiments, the phosphorescence intensities and the kinetic curve of the filter paper were measured with a bifurcated optical fiber system (QBIF600-UV-VIS, Ocean Optics) and collected by a CCD image sensor (QE65000, Ocean Optics). The setup apparatus was shown in Figure S11. In this approach, a 532 nm diode laser (DPGL-2100F, Photop) was used as the excitation source, with an edge filter with a cut-off wavelength of 550 nm throughout the measurement. The beam size is 2 mm. The measurement was done on paper-based sensor. The fiber-optic data were collected every 100 ms for 30 s.

Analysis of glucose sensing efficiency

The efficiency of an optical glucose sensor can be examined simultaneously according to several properties: the increase in relative phosphorescence intensity (ΔI), the phosphorescence change rate, and the time point of inflection in the curve (t_{max}). The phosphorescence change rate can be expressed as the eqn (1), where I_t is phosphorescence intensity at time t, I_0 and I_1 are the phosphorescence intensities at the beginning and at reaching saturation, respectively, and *dt* is the time range for the most significant phosphorescence changes.

Acknowledgement

This work was supported by the Ministry of Science and Technology, Taiwan.

Notes and references

Department of Chemistry, Soochow University, Taipei 111, Taiwan. Fax: +886 (2) 2881 1053; Tel: +886 (2) 2881 9471 ext. 6827; E-mail: meilin_ho@scu.edu.tw

View Article Online
DOI: 10.1039/C7DT00875A

† Electronic Supplementary Information (ESI) available: The sensor scheme, the measurement setup, size distributions, volume, the absorbance of the Ag@Au nanoprisms and Au nanoparticles, and concentration and pH of the buffer, content of the enzyme, the relative emission intensity of the sensor with and without Ag@Au nanoprisms, storage stability test of biosensor, and the comparison of various NP-based glucose sensors. See DOI: 10.1039/b000000x/

1 W. Dong, X. Liu, W. Shi and Y. Huang, *RSC Adv.*, 2015, **5**, 17451-17457.
2 L. Rastogi, A. J. Kora and A. J, *Mater. Sci. Engineer*, 2012, **32**, 1571-1577.
3 H.-C. Wang and A.-R. Lee, *J. Food. Drug. Anal.*, 2015, **23**, 191-200.
4 X.J. Wu and M.M.F. Choi, Topics in Fluorescence Spectroscopy-Glucose Sensing, first ed., Springer US 11, 2006.
5 J.C. Pickup, F. Hussain, N.D. Evans, O.J. Rolinski and D.J.S. Birch, *Biosens. Bioelectron.*, 2005, **20**, 2555-2565.
6 A. Lobnik, M. Turel and Š.K. Urek, *Advances in Chemical Sensors*, first ed., InTech, New York, 2012.
7 D.C. Klonoff, *J. Diabetes Sci. Technol.*, 2012, **6**, 1242-1250.
8 M. Mortellaro and A. DeHennis, *Biosens. Bioelectron.*, 2014, 61, 227-231.
9 G. Srinivasan, J. Chen, J. Parisi, C. Brückner, X. Yao and Y. Lei, *Appl. Biochem. Biotechnol.*, 2015, **177**, 1115-1126.
10 S. Basiruddin and S.K. Swain, *Mater. Sci. Eng. C*, 2016, **58**, 103-109.
11 G.-L. Wang, X.-L. Hu, X.-M. Wu and Z.-J. Li, *Sens. Actuators, B*, 2014, **205**, 61-66.
12 P. Wu, Y. He, H.-F. Wang and X.-P. Yan, *Anal. Chem.*, 2010, **82**, 1427-1433.
13 Y. Li, X. Liu, H. Yuan and D. Xiao, *Biosens. Bioelectron.*, 2009, **24**, 3706-3710.
14 G. Chang, Y. Tatsu, T. Goto, H. Imaishi and K. Morigaki, *Talanta*, 2010, **83**, 61-65.
15 M.-L. Ho, J.-C. Wang, T.-Y. Wang, C.-Y. Lin, J.F. Zhu, Y.-A. Chen and T.-C. Chen, *Sens. Actuators, B*, 2014, **190**, 479-484.
16 C. Lv, W. Di, Z. Liu, K. Zheng and W. Qin, *Analyst*, 2014, **139**, 4547-4555.
17 Y.-A. Chen, F.-J. Tsai, Y.-T. Zeng, J.-C. Wang, H.-L. Chung, S.-Y. Lin, C.P. Hong, P.-H. Huang and G.-H. Lee, *JCCS*, 2016, **63**, 424-431.
18 D. Zeng, W. Luo, J. Li, H. Liu, H. Ma, Q. Huang and C. Fan, *Analyst*, 2012, **137** 4435-4439.
19 A.-L. Hu, Y.-H. Liu, H.-H. Deng, G.-L. Hong, A.-L. Liu, X.-H. Lin, X.-H. Xia and W. Chen, *Biosens. Bioelectron.*, 2014, **61**, 374-378.
20 Y. Tang, Q. Yang, T. Wu, L. Liu, Y. Ding and B. Yu, *Langmuir*, 2014, **30**, 6324-6330.
21 Y. Xianyu and X. Jiang, *Curr. Opin. Chem. Eng.*, 2014, **4**, 144-151.
22 J. Li, Y. Li, S.A. Shahzad, J. Chen, Y. Chen, Y. Wang, M. Yang and C. Yu, *Chem. Commun.*, 2015, **51**, 6354-6356.
23 S. Eustis and M.A. El-Sayed, *Chem. Soc. Rev.*, 2006, **35**, 209-217.
24 Y. Zhang, K. Aslan, S.N. Malyn and C.D. Geddes, *Chem. Phys. B*, 2006, **427**, 432-437.
25 J. Yang, F. Zhang, Y. Chen, S. Qian, P. Hu, W. Li, Y. Deng, Y. Fang, L. Han, M. Luqman and D. Zhao, *Chem. Commun.*,2011, **47**, 11618-11620.
26 K. Munechika, Y. Chen, J.M. Smith and D.S. Ginger, *Metal-Enhanced Fluorescence*, 2010, **17**, 91-118.
27 M.J.R. Previte, K. Aslan, Y. Zhang and C.D. Geddes, *J. Phys. Chem. C*, 2007, **111**, 6051-6059.
28 R. Gill, L. Tian, H.Van Amerongen and V. Subramaniam, *Phys. Chem. Chem. Phys.*, 2013, **15**, 15734-15739.
29 Y. Zhang, K. Aslan, S.N. Malyn and C.D. Geddes, *Chem. Phys. Lett.*, 2006, **427**, 432-437.
30 K.-Y. Cheng, J.-C. Wang, C.-Y. Lin, W.-R. Lin, Y.-A. Chen, F.-J. Tsai, Y.-C. Chuang, G.-Y. Lin, C.-W. Ni, Y.-T. Zeng and M.-L. Ho, *Dalton Trans.*, 2014, **43**, 6536-6547.
31 M.-L. Ho, Y.-P. Yu, Y.-T. Chen and M.-H. Lin, *CrystEngComm*, 2012, **14**, 4049-4059.
32 X.W. Liu, J. Lin, T.F. Jiang, Z.F. Zhu, Q.Q. Zhan and J. Qian, S. He, *Prog. Electromagn. Res.*, 2012, **128**, 35-53.
33 K.-Y. Cheng, J.-C. Wang, C.-Y. Lin, W.-R. Lin, Y.-A. Chen, F.-J. Tsai, Y.-C. Chuang, G.-Y. Lin, C.-W. Ni, Y.-T. Zeng and M.-L. Ho, *Dalton Trans.*, 2014, **43**, 2592-2600.
34 J. Chen, K. Wang, K. Wu, L. Qian, H. Long, B. Wang and P. Lu, *Opt. Commun.*, 2015, **349**, 180-184.
35 W. Liu, H. Wu, B. Li, C. Dong, M. M. F. Choi and S. Shuang, *Anal. Methods*, 2013, **5**, 5154-5460.
36 Y. Zhang, W. Jia, M. Cui, C. Dong, S. Shuang, Y. K. Leung and M. M. F. Choi, *Biotechnol. J.*, 2011, **6**, 492-500.
37 X. Li, Y. Zhou, Z. Zheng, X. Yue, Z. Dai, S. Liu and Z. Tang, *Langmuir*, 2009, **25**, 6580-6586.
38 B. Tang, L. Cao, K. Xu, L. Zhuo, J. Ge, Q. Li and L. Yu, Chemistry, 2008, **14**, 3637-3644.
39 Z. Nie, C.A. Nijhuis, J. Gong, X. Chen, A. Kumachev, A.W. Martinez, M. Narovlyansky and G.M. Whitesides, *Lab Chip*, 2010, **10**, 477-483.
40 Y. Xia, J. Ye, K. Tan, J. Wang and G. Yang, *Anal. Chem.*, 2013, **85**, 6241-6247.
41 N. Fogh-Andersen and P. D'Orazio, *Clin. Chem.*, 1998, **44**, 655-659.
42 E. F. M. Gabriel, P. T. Garcia, T. M. G. Cardoso, F. M. Lopes, F. T. Martins and W. K. T. Coltro, *Analyst*, 2016, **141**, 4749-4756.
43 C. Xue, G.S. Métraux, J.E. Millstone and C.A. Mirkin, *J. Am. Chem. Soc.*, 2008, **130**, 8337-8344.
44 G.S. Métraux and C.A. Mirkin, *Adv. Mater.*, 2005, **17**, 412-415.

TOC

Ag@Au nanoprisms-metal organic frameworks-based paper for enhancing glucose sensing range in human serum and in urine.